IDENTIFICATION OF TWO BRIGHT Z>3 SUBMILLIMETER GALAXY CANDIDATES IN THE COSMOS FIELD*

M. Aravena¹, J. D. Younger^{2,3}, G. G. Fazio⁴, M. Gurwell⁴, D. Espada^{4, 5}, F. Bertoldi⁶, P. Capak⁷, D. Wilner⁴

Draft version October 30, 2018

ABSTRACT

We present high-resolution interferometric Submillimeter Array (SMA) imaging at $890\mu m$ ($\sim 2''$ resolution) of two millimeter selected galaxies – MMJ100015+021549 and MMJ100047+021021 – discovered with the Max-Planck Millimeter Bolometer (MAMBO) on the IRAM 30 m telescope and also detected with Bolocam on the CSO, in the COSMOS field. The first source is significantly detected at the $\sim 11\sigma$ level, while the second source is tentatively detected at the $\sim 4\sigma$ level, leading to a positional accuracy of $\sim 0.2-0.3''$. MM100015+021549 is identified with a faint radio and K-band source. MMJ100047+021021 shows no radio emission and is tentatively identified with a very faint K-band peak which lies at $\sim 1.2''$ from a clumpy optical source. The submillimeter-to-radio flux ratio for MM100015+021549 yields a redshift of ~ 4.8 , consistent with the redshift implied by the UV-to-submillimeter photometry, $z \sim 3.0-5.0$. We find evidence for warm dust in this source with an infrared luminosity in the range $\sim 0.9-2.5\times 10^{13}~L_{\odot}$, supporting the increasing evidence for a population luminous submillimeter galaxies at z>3. Finally, the lack of photometric data for MMJ100047+021021 does not allow us to investigate its properties in detail, however its submillimeter-to-radio ratio implies z>3.5.

Subject headings: galaxies: evolution — galaxies: high-redshift — galaxies: starburst

1. INTRODUCTION

Submillimeter (submm) wavelength blank-field surveys discovered a population of heavily dust-obscured starburst galaxies at high redshifts (e.g. Smail et al. 1997; Barger et al. 1998; Hughes et al. 1998). These submm galaxies (SMGs) contribute a large fraction of the comoving infrared (IR) luminosity density at high-redshift (Le Floc'h et al. 2005), and their clustering properties indicate they could be progenitors of the most massive galaxies at z < 1 (Blain et al. 2004; Viero et al. 2009; Aravena et al. 2010). The number counts and dust production rates of these massive, high-redshift starburst

* Based on observations obtained with the SMA, which is a joint project between the Smithsonian Astrophysical Observatory and the Academia Sinica Institute of Astronomy and Astrophysics and is funded by the Smithsonian Institution and the Academia Sinica. Also based on observations obtained, within the COSMOS Legacy Survey, with: the Institut de Radioastronomie Millimetrique (IRAM) 30 m telescope, the Caltech Submillimeter Observatory (CSO), the APEX telescope, the Hubble Space Telescope (HST), the Spitzer Space telescope, the Subaru telescope, the Kitt Peak National Observatory (KPNO), the Cerro Tololo Inter-American Observatory (CTIO), the National Optical Astronomy Observatory (NOAO), the United Kingdom IR telescope (UKIRT) and the Canada-France-Hawaii telescope (CFHT). The National Radio Astronomy Observatory (NRAO) is a facility of the National Science Foundation operated under cooperative agreement by Associated Universities, Inc.

¹National Radio Astronomy Observatory. 520 Edgemont Road, Charlottesville VA 22903, USA. maravena@nrao.edu

² Institute for Advanced Study, Einstein Drive, Princeton, NJ 08544 USA

³ Hubble Fellow.

⁴ Harvard Smithsonian Center for Astrophysics, 60 Garden St. Cambridge MA 02138 USA

St., Cambridge, MA 02138, USA
⁵ Instituto de Astrofísica de Andalucía - CSIC, Apdo. 3004, 18080 Granada, Spain.

⁶ Argelander Institut für Astronomie. Auf dem Hügel 71,
 53121 Bonn, Germany.
 ⁷ California Institute of Technology, 1200 East California

California Institute of Technology, 1200 East California Boulevard, Pasadena, CA 91125, USA galaxies actually place tight constrains on galaxy formation models (Baugh et al. 2005).

The identification of optical counterparts to the submm sources has mainly been based on the identification of radio counterparts, detected through deep Very Large Array (VLA) 20 cm imaging. This technique exploits the local far-IR/radio correlation (Condon 1992) and statistical arguments to claim an association between a closeby radio source and the submm source, localizing the SMG with an accuracy of $\sim 1''$. The direct search for counterparts in optical wavebands is not practical due to their common faintness and the high number density of optical sources within the positional uncertainty. For about 70-80% of all submm sources precise positions can be determined from an identification of faint radio counterparts (Ivison et al. 2007).

However, the depth of current radio observations limits the identification of submm sources to z < 3, since due to the strong K-correction, the radio flux (unlike the submm flux) drops rapidly with redshift (Carilli & Yun 1999). The only unambiguous way to localize the highest-redshift SMGs in the optical/near-IR is via submm interferometry.

Radio-selected SMGs have been found to have a median redshift of z=2.3 (Chapman et al. 2005). However, recent interferometric submm imaging of a flux-limited sample of SMGs has provided substantial evidence that up to $\sim 30\%$ of this population is likely located at z>3 (Iono et al. 2006; Younger et al. 2007, 2009). These radio-dim SMGs appear to be inconspicuous at optical wavelengths, likely obscured by large amounts of dust, and their nature can only be revealed in the IR (Wang et al. 2007; Dannerbauer et al. 2008; Cowie et al. 2009). To date, only five such high-redshift SMGs have been confirmed spectroscopically (Capak et al. 2008; Schinnerer et al. 2008; Coppin et al.

2 M. Aravena

Band	λ^b	MM1	MM14S	MM14N	Units
B^+	0.45	< 21	< 21	24 ± 7	пJу
i^+	0.77	56 ± 16	< 35	116 ± 11	nJy
$K_{ m S}$	2.2	768 ± 77	222 ± 160	340 ± 140	nJy
IRAC	3.6	1.3 ± 0.2	< 0.2	0.20 ± 0.06	$\mu \mathrm{Jy}$
IRAC	4.5	1.9 ± 0.3	< 0.3	0.32 ± 0.11	$\mu \mathrm{Jy}$
MIPS	24		< 0.06	< 0.06	mJy
MIPS	70	< 2.1	< 2.7	< 2.7	mJy
MIPS	160	< 15	< 15	< 15	mJy
LABOCA	870	16.4 ± 1.8	< 10.5		mJy
SMA	890	16.8 ± 1.5	8.5 ± 2.0	< 6	mJy
Bolocam	1100	6.9 ± 1.9	3.8 ± 19		mJy
MAMBO	1200	6.2 ± 0.9	4.1 ± 1.0		mJy
VLA	20	35 ± 10	< 30	< 30	$\mu \mathrm{Jy}$

TABLE 1 Multi-wavelength photometry a

2009; Daddi et al. 2009b,a; Knudsen et al. 2010).

In this paper, we report accurate astrometry of two bright SMGs in the COSMOS field whose radio to submm flux ratio indicates that are likely at z > 3. We assume a standard cosmology with $H_0 = 71$ km s⁻¹ Mpc⁻¹, $\Omega_{\Lambda} = 0.73$ and $\Omega_{\rm M} = 0.27$.

2. OBSERVATIONS

2.1. The COSMOS field

COSMOS is the largest deep survey carried out with the *Hubble Space telescope* (HST) covering $\sim 2~{\rm deg^2}$ in the sky. Extensive imaging of the COSMOS field has been performed from the X-rays to the radio wavelengths. This includes: complete optical/near-IR coverage in 22 broad and intermediate bands with several ground based observatories including the Subaru telescope, the CFHT, the UKIRT and the KPNO; IR imaging with *Spitzer*, including new deep 3.6 and 4.5 μ m images obtained as part of its warm mission; and radio imaging with the VLA at 20 cm. For details in the optical/IR imaging and catalogs of the COSMOS field see Capak et al. (2007) and Ilbert et al. (2009). A complete description of the radio imaging is given in Schinnerer et al. (2007).

2.2. Sample selection

In the course of the MAMBO 1.2 mm survey of the COSMOS field (Bertoldi et al. 2007), fifteen sources were detected with S/N > 4, five of which do not have a significant radio counterpart (< 30 μ Jy, 3σ). From these five radio-faint mm sources, we selected two that were also significantly detected at 1.1 mm with Bolocam: MMJ100016+021549 and MMJ100047+021018. Hereafter, we refer to these sources as MM1 and MM14, respectively, following Bertoldi et al. (2007). The deboosted flux densities for MM1 were $S_{1.2\text{mm}}=6.2\pm0.9$ mJy and $S_{1.1\text{mm}}=5.9\pm1.9$ mJy in the MAMBO and Bolocam maps, respectively (Bertoldi et al. 2007). This source was recently detected with the Large Bolometer Camera (LABOCA) with $S_{870\mu\text{m}}=16.4\pm1.8$ mJy (Albrecht et al., in preparation). The MAMBO and Bolocam deboosted flux densities for MM14 were $S_{1.2\text{mm}}=$

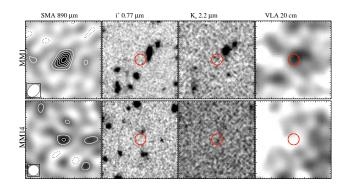


Fig. 1.— Postage stamps centered at the position of the SMA detections. Images are $14''\times14''$ in size. The images to the left show the SMA 890 $\mu \rm m$ emission at significance levels of -4, -2, 2, 4, 6, 8 and 10σ (see text). Solid and dashed contours represent positive and negative fluxes, respectively. The red 2'' diameter circle represents the position of the SMA detection.

 4.1 ± 1.0 mJy and $S_{1.1\text{mm}} = 3.6 \pm 1.9$ mJy, respectively (Bertoldi et al. 2007), however no significant emission is seen in the LABOCA image down to 10.5 mJy ($\sim 3\sigma$).

2.3. $SMA~890~\mu m~imaging$

SMA observations of MM1 and MM14 were carried out in 2009 January 10 and 2009 May 07, respectively, under good weather conditions ($\tau_{250\mathrm{GHz}} < 0.1$). The receivers have two sidebands, each with 2 GHz bandwidth, which when averaged yield a 4 GHz effective bandwidth centered at 345 GHz ($\lambda \sim 890~\mu\mathrm{m}$). Seven antennas, arranged in the compact (COM) configuration⁹ with the MAMBO source positions as phase tracking centers.

The data were calibrated with the MIR package (Scoville et al. 1993) specially adapted for SMA data, using the strong continuum source 3C273 ($S_{345GHz} \sim 4.9$ Jy) as passband calibrator and Ceres ($S_{345GHz} \sim 4.2$ Jy) for primary flux calibration. The flux scale is estimated to be accurate within 20%. The quasars J0854+201 (~ 3.1 Jy; $\sim 24.2^{\circ}$ away) and J1058+015 (~ 1.7 Jy; $\sim 14.5^{\circ}$ away) were observed every ~ 25 min for gain calibration. Following Younger et al. (2008, 2009, 2010), we also performed hourly scans of a dimmer, but significantly closer test quasar J1008+063 (~ 0.11 Jy; $\sim 4.5^{\circ}$ away) to empirically verify the phase transfer and estimate the positional uncertainty. The visibility data for MM1 showed good phase stability, however, about half of the data for MM14 had to be flagged due to bad phases.

The calibrated visibility data were imaged using the AIPS software. We used the AIPS task IMAGR, which uses the CLEAN algorithm, and natural weighting to deconvolve the images down to 1σ in a box centered on our targets. This led to beam sizes of $2.55'' \times 1.86''$ and $1.96'' \times 1.86''$ and noise levels of 1.5 mJy and 1.95 mJy beam⁻¹ for MM1 and MM14, respectively. Finally, fluxes were measured with Gaussian fits using the JMFIT task, included in the AIPS software.

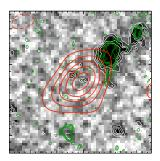
3. RESULTS AND ANALYSIS

3.1. SMA detections

Fitting two-dimensional Gaussians to the SMA images, leads to flux densities of 16.8 ± 1.5 mJy and 8.5 ± 2.0 mJy

 9 half-power beam width (HPBW) $\approx 2^{\prime\prime};$ see http://sma1.sma.hawaii.edu/specs.html for more information.

 $[^]a$ Measurements at 3.6 and 4.5 $\mu{\rm m}$ based on the deep Spitzer warm mission exposures. b Wavelength in microns, except for the VLA where it is given in centimeters. c Photometry in the MIPS 24 $\mu{\rm m}$ bands not possible due to blending with a bright source.



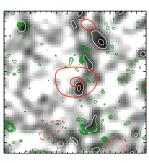


Fig. 2.— K-band $8'' \times 8''$ postage stamp images centered at the position of the SMA detections of MM1 (left) and MM14 (right), with K-band white contours overlaid at 2, 3, 4 and 5σ levels. Green contours represent the HST F814W image smoothed with a Gaussian kernel of 3 pixels (0.15'') at 2, 3, 4 and 5σ levels. The red contours represent the 890 μ m emission with levels as in Fig. 1. The K-band image for MM14 has also been smoothed with a Gaussian kernel of 3 pixels (0.45'') to enhance the significance level.

for MM1 and MM14, respectively. The MM14 detection is tentative since, as we shall see below, it could not be reliably identified with any significant counterpart at other wavelengths.

The Gaussian fit indicates that both sources are unresolved with a maximum deconvolved FWHM size of $1.8'' \times 1.0''$ and $2.0'' \times 0.6''$, respectively, consistent with the sizes found for high-redshift SMGs, which are typically unresolved at $\sim 2''$ resolution (Iono et al. 2006; Younger et al. 2007; Wang et al. 2007; Younger et al. 2009). This also yields from the flatness of the real visibility amplitudes as a function of the projected baseline length. The measured SMA position for MM1 is $\alpha(J2000) = 10^{h}00^{m}15.612^{s}, \delta(J2000) = +02^{\circ}15'49.00'',$ with a positional error in the Gaussian fit of 0.09", while for MM14 it is $\alpha(J2000) = 10^{h}00^{m}47.329^{s}, \delta(J2000) =$ $+02^{\circ}10'21.44''$, with a positional error in the fit of 0.15''. This positional accuracy in the fit is consistent with the one expected for the beam and S/N of the observations: 0.09" and 0.2" for MM1 and MM14, respectively. From the comparison of the reference (Browne et al. 1998) and measured (this work) positions of the test quasar J1008+063, we find a positional uncertainty of 0.18''. This, added in quadrature to the positional error in the Gaussian fit to the MM1 and MM14 images, gives a positional uncertainty of 0.2'' and 0.27'', respectively.

3.2. Multi-wavelength counterparts

MM1. The SMA peak position coincides with the position of a $\sim 3.5\sigma$ radio peak (Fig. 1). A bright and elongated source with photometric redshift z = 1.4(Ilbert et al. 2009) is located at ~ 2.1 "north-west from the SMA position. The radio peak lies within 0.3" from the SMA position, however given the beam of the radio image ($\sim 2''$), we do not discard that part of the emission comes from this bright optical source. From Fig. 2 (left), we identify a very faint K-band source, located at $\approx 0.3''$ from the SMA position, as the likely counterpart. The bright optical source strongly contaminates the Spitzer images, making it difficult to reliably measure the faint emission of MM1. We extracted photometry in the IRAC bands by subtracting this bright source based on the Kband image convolved with the IRAC PSF (Table 1). We do not attempt to extract photometry of this source in the 24 μ m images. No emission is detected at 70 and 160 μm .

The deep K-band images show two peaks, separated by about 0.6", or a physical scale of ~ 4.3 kpc at $z \sim 3$ (Fig. 2). The fainter peak appears to be the one associated with the submm emission, suggesting a possible double system, similar to the case of the SMG AzTEC11 (Younger et al. 2009).

MM14. The radio maps do not show any peak close to the position of the SMA source down to a 3σ level of 30 μ Jy. At $\sim 1.2''$ to the north of the SMA position we find a faint optical source that appears diffuse and faint in the K-band (Fig. 1). This source has a likely photometric redshift of ~ 3.4 (Mobasher et al. 2007).

From Fig. 1, the northern optical source appears to be composed by several "clumps" that extend over $\sim 1.5''$ or ~ 11 kpc at $z \sim 3.5$. We also find a very faint Kband emission peak ($\sim 3\sigma$ in the smoothed image), located 0.4'' to the south of the SMA position (Fig. 2). This peak has $\sim 2\sigma$ significance in the original K-band image (without smoothing; Fig. 1), implying the source is spatially extended. Due to its proximity to the SMA position, it appears to be the most likely counterpart to the submm emission despite its faintness. Hereafter, we refer to this source as MM14S (south), while for the northern optical source we refer as MM14N. However, since we could not reliably identify any significant multiwavelength counterpart for this source and given the relatively low significance of the SMA detection, we label this source (MM14S) as a tentative detection.

The spatial configuration between MM14S and MM14N could resemble a merger/interaction system, where the submm emission comes from a highly obscured source (MM14S), but could also correspond to an extended galaxy with the submm emission located in an obscured spiral arm. The offset between the MM14N and the submm position (MM14S) is ~ 9 kpc, assuming $z \sim 3.5$, similar to the case of the high-redshift SMG GN20 (Iono et al. 2006), where the submm and the optical peaks are separated by $\sim 0.8''$, or ~ 6 kpc. Based on the local density of sources with z > 3, n = 0.002 arcsec⁻², we find that the probability that a z > 3 optical source brighter than MM14N is located by chance within a distance of 1.2" from the SMA position is only P = 0.9%, thus supporting a physical association.

Optical/IR photometry was performed with SExtractor (Bertin & Arnouts 1996) in a 2" aperture, using the K-band images for detection. None of our targets was detected in the Spitzer MIPS bands, and we thus provide 3σ upper limits based on their local noise level within one beam. The measured flux densities at several wavelengths for MM1, MM14S and MM14N are listed in Table 1.

3.3. Photometric redshifts

MM1 and MM14S were not detected in the COSMOS catalogs (Capak et al. 2007; Ilbert et al. 2009) and thus there is no previous estimate for their redshift.

Assuming that the correlation between the far-IR and radio integrated emission from local starburst galaxies also holds for distant galaxies, the submm-to-radio flux ratio can be used as a measure of redshift (Carilli & Yun 1999). Figure 3 shows the 890 μ m to 20 cm flux ratio as a function of redshift for the prototypical starburst galaxy Arp220, and illustrates the uncertainties introduced by

4 M. Aravena

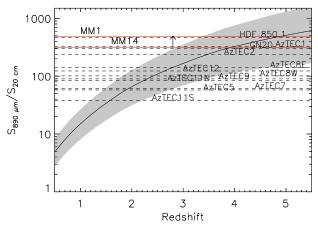


FIG. 3.— Redshift estimation based on the submm-to-radio flux ratio. The solid line represents this ratio computed for the IR luminous starburst galaxy Arp220 (which roughly has $T_{\rm dust}=45$ K). The filled area shows the flux ratio obtained for similar models with dust temperatures from 30 to 60 K. Dashed horizontal lines show the flux ratios measured for the radio-identified submm sources with SMA detections (Younger et al. 2007, 2009), and for the high-redshift SMGs HDF 850.1 and GN20 (Cowie et al. 2009; Iono et al. 2006). The upper pointing arrow represents the lower limit in the flux ratio for MM14S.

different dust temperatures. From this, we derive a redshift of $4.8^{+2.5}_{-1.4}$ for MM1, and a lower limit z>3.5 for MM14S.

Given the lack of optical/IR photometric information for MM14S, we do not attempt to derive the redshift and dust properties of this source, and hereafter we focus on MM1 and MM14N.

We derived optical/IR photometric redshifts for MM1 and MM14N using the HyperZ code (Bolzonella et al. 2000). We allowed for a redshift range z=0-7, and using a Calzetti et al. (2000) extinction law with an extinction range $A_{\rm V}=0-4$. For comparison, we used two different set of templates libraries: 5 solar metallicity stellar population models from Bruzual & Charlot (2003), similar to the HyperZ defaults; and 10 templates from the SWIRE library (Polletta et al. 2007), including models for an elliptical, three spiral, four starburst and three AGN dominated galaxies.

As shown in Fig. 4, the χ^2 distribution and redshift solutions for MM1 and MM14N obtained using both set of templates are similar. Using the Bruzual & Charlot (2003) templates, the best fit for MM1 is produced at $z=3.1^{+0.5}_{-0.6}$ by a spiral galaxy model, with $A_{\rm V}=1.4$ (black curve); while the best fit for MM14N is produced at $z=3.7^{+0.3}_{-0.3}$ by a single burst model, with $A_{\rm V}=1.0$. Using the SWIRE library, the best fits are produced by a late spiral galaxy at $z=3.0^{+0.5}_{-0.9}$ and a QSO template at $z=3.6^{+0.2}_{-0.3}$ for MM1 and MM14N, respectively. The quoted uncertainties correspond to the 90% confidence level derived from the fitting routine.

Each of the Bruzual & Charlot (2003) templates follow a prescription for the stellar mass to luminosity ratio (e.g. as a function of age). Using the best fits and assuming a Chabrier (2003) initial mass function, we find stellar masses of $\sim 1.0 \times 10^{11}~M_{\odot}$ and $\sim 3.6 \times 10^{10}~M_{\odot}$, for MM1 and MM14N, respectively. We note, however, that these stellar mass estimates are rough given the large uncertainty in redshift.

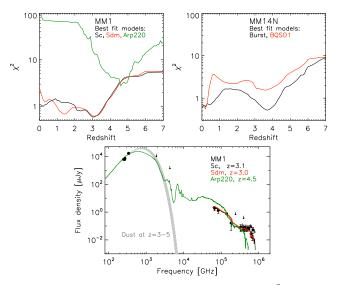


FIG. 4.— Photometric redshift results. Top: the χ^2 values as a function of redshift obtained by fitting the optical photometry with the the Bruzual & Charlot (2003) templates (black curves) and the SWIRE templates (red curves) for MM1 (left) and MM14N (right); and by fitting the UV-to-mm photometry with the SWIRE templates (green curves) for MM1. Bottom: SED of MM1. The colors represent the different template libraries used. The gray curve shows the best fit dust model to the far-IR data at z=3-5.

For MM1, we also computed redshifts by fitting templates to the UV-to-mm photometry. We used the same SWIRE templates, redshift and extinction ranges. The best fit is produced by an Arp220 model, with $A_{\rm V}=0.3$ and z=4.5. The value of χ^2 is dominated by the ratio between the submm to optical light, indicating a possible range of redshift from ~ 3.0 to 5.0. Our redshift estimates are in good agreement with the redshift implied by the submm to radio flux ratio and supports a higher redshift than that obtained purely from the optical photometry.

3.4. Dust properties

As illustrated in Fig. 4, the far-IR SED of MM1 can be described by a modified black body spectrum. We fitted a model of the form $S_{\nu} \propto B_{\nu}(T_{\rm dust})(1-e^{-\tau_{\nu}})$, where $B_{\nu}(T_{\rm dust})$ is the Planck function. The opacity, τ_{ν} , is proportional to the dust mass $M_{\rm dust}$ and to ν^{β} , with the emissivity index $\beta = 1.5$. Given the large uncertainties in redshift, we consider a range of redshift z = 3 - 5 to model the photometric data $(70 - 1200 \mu {\rm m})$.

We find dust temperatures and masses in the range $T_{\rm dust} = 50-65~{\rm K}$ and $M_{\rm dust} = 1.2-2.6\times 10^9~M_{\odot}$. These models imply far-IR luminosities $L_{8-1000\mu{\rm m}} = 0.9-2.5\times 10^{13}~L_{\odot}$. Using the computed IR luminosities and the Kennicutt (1998) empirical calibration, we compute star-formation rates (SFRs) of $1800-5000~M_{\odot}~{\rm yr}^{-1}$ for this source.

4. DISCUSSION

Our detection of two out of the five significant radiofaint sources discovered in the MAMBO survey of the COSMOS field supports the increasing evidence for a population of luminous SMGs at z>3. It has recently been suggested that these galaxies may be the progenitors of quiescent, massive galaxies at $z\sim2$ (Capak et al. 2008; Coppin et al. 2009, 2010). The old stellar populations found in these $z\sim 2$ quiescent galaxies require to have formed at z>3 in short bursts of star formation.

If we assume that four of these five MAMBO sources with no radio significant radio counterparts are real and located at z>3 (e.g., we expect that one of the five is a fake detection due to flux boosting), it implies that up to $\sim 30\%$ (4/15) of the $S_{250{\rm GHz}}>4$ mJy detections are located at z>3. This is well justified by the confirmation of MM1 and tentative detection of MM14 with the SMA, and of two other MAMBO sources with LABOCA (Albrecht et al., in preparation). Assuming that 2-4 of the MAMBO sources are uniformly distributed over the comoving volume spanned by z=3-5 within the area of the MAMBO survey, we find a surface density of $\sim 13-30~{\rm deg}^{-2}$ and a volume density of $\sim 1-6\times 10^{-6}$

 ${
m Mpc^{-3}}$. This is consistent with the upper limit of $> 10^{-6}$ ${
m Mpc^{-3}}$ (> 6 deg⁻²) from the spectroscopically confirmed z>4 SMGs (Coppin et al. 2009) and with the density of $z\sim3-5$ systems with baryonic masses $>10^{11}~M_{\odot}$ from predictions of theoretical models (Baugh et al. 2005).

JDY acknowledges support from NASA through Hubble Fellowship grant #HF-51266.01 awarded by the Space Telescope Science Institute, which is operated by the Association of Universities for Research in Astronomy, Inc., for NASA, under contract NAS 5-26555. DE was supported by a Marie Curie International Fellowship within the 6th European Community Framework Programme (MOIF-CT-2006-40298).

REFERENCES

Aravena, M., et al. 2010, ApJ, 708, L36
Barger, A. J., Cowie, L. L., Sanders, D. B., Fulton, E., Taniguchi, Y., Sato, Y., Kawara, K., & Okuda, H. 1998, Nature, 394, 248
Baugh, C. M., Lacey, C. G., Frenk, C. S., Granato, G. L., Silva, L., Bressan, A., Benson, A. J., & Cole, S. 2005, MNRAS, 356, 1191
Bertin, E. & Arnouts, S. 1996, A&AS, 117, 393
Bertoldi, F., et al. 2007, ApJS, 172, 132
Blain, A. W., Chapman, S. C., Smail, I., & Ivison, R. 2004, ApJ, 611, 725
Bolzonella, M., Miralles, J., & Pelló, R. 2000, A&A, 363, 476
Browne, I. W. A., Wilkinson, P. N., Patnaik, A. R., & Wrobel, J. M. 1998, MNRAS, 293, 257
Bruzual, G., & Charlot, S. 2003, MNRAS, 344, 1000
Calzetti, D., Armus, L., Bohlin, R. C., Kinney, A. L., Koornneef, J., & Storchi-Bergmann, T. 2000, ApJ, 533, 682
Capak, P., et al. 2007, ApJS, 172, 99
— 2008, ApJ, 681, L53
Carilli, C. L., & Yun, M. S. 1999, ApJ, 513, L13
Chabrier, G. 2003, ApJ, 586, L133
Chapman, S. C., Blain, A. W., Smail, I., & Ivison, R. J. 2005, ApJ, 622, 772
Condon, J. J. 1992, ARA&A, 30, 575
Coppin, K., et al. 2010, arXiv:1004.4001
— 2009, MNRAS, 395, 1905
Cowie, L. L., Barger, A. J., Wang, W., & Williams, J. P. 2009, ApJ, 697, L122
Daddi, E., Dannerbauer, H., Krips, M., Walter, F., Dickinson, M., Elbaz, D., & Morrison, G. E. 2009a, ApJ, 695, L176

Daddi, É., et al. 2009b, ApJ, 694, 1517

Dannerbauer, H., Walter, F., & Morrison, G. 2008, ApJ, 673, L127
Greve, T. R., et al. 2005, MNRAS, 359, 1165
Hughes, D. H., et al. 1998, Nature, 394, 241
Ilbert, O., et al. 2009, ApJ, 690, 1236
Iono, D., et al. 2006, ApJ, 640, L1
Ivison, R. J., et al. 2007, MNRAS, 380, 199
Kennicutt, Jr., R. C. 1998, ARA&A, 36, 189
Knudsen, K. K., Kneib, J., Richard, J., Petitpas, G., & Egami, E. 2010, ApJ, 709, 210
Le Floc'h, E., et al. 2005, ApJ, 632, 169
Michalowski, M. J., Watson, D., & Hjorth, J. 2010, ApJ, 712, 942
Mobasher, B., et al. 2007, ApJS, 172, 117
Polletta, M., et al. 2007, ApJ, 663, 81
Schinnerer, E., et al. 2007, ApJS, 172, 46
— 2008, ApJ, 689, L5
Scoville, N. Z., Carlstrom, J. E., Chandler, C. J., Phillips, J. A., Scott, S. L., Tilanus, R. P. J., & Wang, Z. 1993, PASP, 105, 1482
Smail, I., Ivison, R. J., & Blain, A. W. 1997, ApJ, 490, L5+
Viero, M. P., et al. 2009, ApJ, 707, 1766
Wang, W., Cowie, L. L., van Saders, J., Barger, A. J., & Williams, J. P. 2007, ApJ, 670, L89
Younger, J. D., et al. 2007, ApJ, 671, 1531
— 2008, ApJ, 688, 59
— 2009, ApJ, 704, 803
— 2010, arXiv:1003.4264